Document Version:

This is the Accepted Manuscript version.
The version in the University of Hertfordshire Research Archive may differ from the final published version.

Enquiries

If you believe this document infringes copyright, please contact Research & Scholarly Communications at rsc@herts.ac.uk

Coupled Cooling Method and Application of Latent Heat Thermal Energy Storage Combined with Pre-cooling of Envelope: Optimization of Pre-cooling with Intermittent Mode

Gao Xiangkui[1] *Yuan Yanping**[1] *Wu Hongwei*[2] *Cao Xiaoling*[1] *Zhao Xudong*[3]

[1]School of Mechanical Engineering, Southwest Jiaotong University, 610031 Chengdu, China

[2]School of Engineering and Technology, University of Hertfordshire, Hatfield, AL10 9AB, United Kingdom

[3]School of Engineering, Faculty of Science, University of Hull, Hull, HU6 7RX, United Kingdom

Highlights

- An intermittent operational mode for PE of the new coupled cooling system is proposed.

- A simplified numerical model of intermittent cold storage is established.

- PE is divided into two periods, with their own respective evaluation indices proposed.

- An interchanging continuous/intermittent cold storage strategy is proposed.

- Energy consumption can be reduced by 68–78% as compared to the continuous mode.

Abstract：The coupled cooling method combining latent heat thermal energy storage and pre-cooling of the envelope (PE) is a new free-cooling method that is suitable for exposure to high temperatures and other types of harsh environments. PE plays the most critical role in the coupled cooling method. Long-term, continuous PE cannot only reduce energy storage capacity, but it also causes numerous energy waste. Thus, an intermittent operational mode is firstly proposed to improve the heat transfer performance and reduce energy consumption. A simplified numerical model of intermittent thermal storage is established, and the subsequent effects of intermittent ratio (IR) and intermittent period (IP) on cold storage performance have been systematically investigated. Furthermore, the operational period is divided into a cold storage period (CSP) and a cold preservation period (CPP), each with their own respective evaluation indices. Long-term intermittent PE is optimized, and an interchanging continuous/intermittent cold storage strategy is proposed. Under the current operating conditions, as compared with the conventional continuous mode, the duration of CSP is extended by 0–26%, yielding an annual cold storage energy

consumption reduction of 68–78%. Thus, the current study demonstrates the significant potential

of intermittent operational mode application in underground thermal energy storage systems.

Key words: Underground space; Mine refuge chamber; Thermal energy storage; Cavern envelope;

Intermittent operation; Optimization

Nomenclature

A	area, m^2
c_P	specific heat, J/(kg·K)
h	convective heat transfer coefficient, W/(m^2·K)
H	height, m
L	length, m
n	non-negative integer
r	radius, m
t	Celsius temperature, ℃
T	thermodynamic temperature, K
W	width, m

Greek symbols

α	thermal diffusivity, m^2/s
φ	evaluation parameter for CPP
Δ	difference
λ	thermal conductivity, W/(m·K)
τ	time, s
ρ	density, kg/m^3
υ	viscosity, m^2/s
Θ	dimensionless target cold storage temperature

Subscripts

c	cold storage
f	flow air
i	inner/indoor
ina	inactive
n	net
∞	far boundary
ope	operation
R	refuge chamber
$R1$	side wall of refuge chamber
$R2$	vault of refuge chamber
tcs	target cold storage
w	wall
$Upper$	upper value

Abbreviations

CPP   Cold preservation period

CSP   Cold storage period

CTES   Cavern thermal energy storage

IP   Intermittent period

IR   Intermittent ratio

LHTES Latent heat thermal energy storage

PCM   Phase-change material

PE   Pre-cooling of the envelope

SIMPLE Semi-implicit method for pressure-linked equations

SR   Surrounding rock

TES   Thermal energy storage

UTES   Underground thermal energy storage

Dimensionless numbers

Bi   Biot number

Fo   Fourier number

1. Introduction

Recently, renewable energy has been attracting great attention as energy consumption and carbon emissions have significantly increased. Efficient usage of renewable energy requires reliable thermal energy storage (TES) because a disparity exists in time and space between the amount of energy generated via energy sources and user demands [1,2]. It is known that energy sources such as solar energy, geothermal energy, industrial waste heat, groundwater, and snow do not require energy conversion prior to being stored via TES [3,4]; the TES system is subsequently able to release energy when heating or cooling is required.

CTES is one type of underground thermal energy storage (UTES) [5] that uses the surrounding rock (SR) of caverns as the energy storage tank. As compared with the two remaining types of UTES, which are aquifer thermal energy storage and borehole thermal energy storage, the structure of CTES is more stable, permitting adaptation to different underground environments [6]. In addition, in contrast to above-ground thermal energy storage technology, it offers flexible design options and can be stored at various temperatures without affecting the weather and climate, thereby making CTES more suited to meet industrial requirements [7]. Park et al. [5] performed a numerical study on the reliability of high-temperature energy storage in CTES and compared the results with those of ground thermal energy storage. It was found that the amount of heat loss in the CTES system was significantly lesser than that in the ground thermal energy storage system.

3

Ghoreishi-Madiseh et al. [6] developed three-dimensional (3D) numerical models to study large-scale rock-pit seasonal TES for application in underground mine ventilation. Their results suggested that seasonal TES of rock-pit was able to reduce energy consumption during heating in winter and cooling in summer.

There are still numerous problems with CTES, such as its low-energy utilization rate. In addition, with the decrease in the heat transfer temperature difference over the operational period, the energy utilization rate is further reduced. However, an intermittent operational strategy could effectively solve this problem by accelerating the recovery of the temperature difference to ensure that the SR is able to absorb and store energy. Current research on UTES with an intermittent mode mainly focuses on heat recovery performance enhancement in the ground heat exchanger, which is a single component of the ground source heat pump system. Shang et al. [8,9] presented a 3D model of the ground heat exchanger to study the geo-temperature variation by implementing an intermittent operational mode; additionally, the effects of control factors such as thermal conductivity, backfill material, porosity, solar radiation energy, air temperature, and velocity of wind on the soil recovery process were investigated. Their results showed that the soil properties played a significant role in heat recovery, whereas the environmental factors yielded negligible influence. Cao et al. [10,11] developed an integrated numerical and theoretical heat transfer model of a ground heat exchanger system. The impact of different intermittent ratios on the heat transfer performance of a vertical buried tube was investigated. It was concluded that the intermittent operational mode could effectively enhance the heat transfer performance of a ground heat exchanger system. In addition, Liu et al. [12] reached a similar conclusion upon studying the heat transfer performance of a ground heat exchanger in a direct refrigeration system with an intermittent mode. When Faizal et al. [13,14] conducted an experimental study to investigate the heat transfer performance of a ground heat exchanger with an intermittent operational mode, it was found that operational durations of 8 h and 16 h within a 24 h period could increase the energy gain by 40.9% and 14.8%, respectively, as compared to the mode of 24 h continuous operation.

To the best of the knowledge of the authors, to-date research on UTES systems that implement intermittent modes primarily focus on soil heat recovery in the ground heat exchanger of borehole thermal energy storage systems. However, because the heat transfer medium of CTES includes the indoor air and cavern envelope, which significantly differs from the ground heat

4

exchanger, the requirements of CTES and ground heat exchangers are substantially dissimilar.

Fig. 1. Interior of a typical permanent refuge chamber.

Fig. 1 shows an underground emergency mine rescue shelter [15], which is purposed as a safe place for trapped miners to await rescue. In the event of a mining accident, depending on the internal and environmental conditions, the refuge chamber may become an isolated, hot, and humid space with no power supply. In China, while the base temperature of a mine refuge chamber is typically higher than 30℃, in the absence of an external power supply, the temperature in a refuge chamber must not exceed 35℃ within 96 h [16].

As illustrated in Table 1, it can be concluded that each of the existing cooling methods, which include CO_2 phase-change cooling, explosion-proof electrical air conditioning, ventilation cooling, and ice storage cooling, have their own limitations [17]. In addition, the latent heat thermal energy storage (LHTES) system is also unable to autonomously regulate the temperature because of the large cold loads or small operating temperature difference between the high base temperature and relatively low maximum temperature.

(a)   (b)
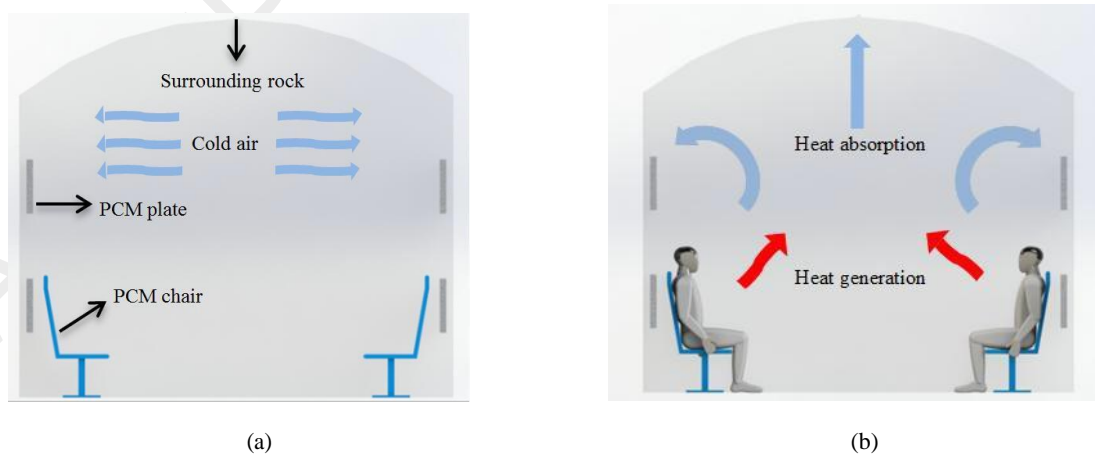
Fig. 2. Schematic of proposed coupled cooling method: (a) PE during peacetime; (b) heat storage of LHTES and

envelope during working time.

To solve this problem, a new coupled cooling method implementing LHTES and pre-cooling of the envelope (PE) has been proposed by the authors, Yuan and Gao et al [17,18]. As shown in Fig. 2(a), the envelope is pre-cooled via a forced-air system during peacetime; as this occurs, the phase-change material (PCM) absorbs and stores the cool air in units placed within the chamber. As shown in Fig. 2(b), when mine accident happened, the temperature can be regulated by making full use of the sensible heat storage capacity of the envelope and latent heat storage capacity of the PCM without power.

PE can not only increase the operating temperature difference (i.e., the temperature difference between the base and maximum temperatures) of the PCM, but it is also able to sustain heavy cold loads to reduce the required amount of PCM. This coupled cooling method is able to meet safety requirements, requires no power during working time, is stable and reliable under various conditions, and widens the application range of the LHTES system with respect to temperature control. Furthermore, energy can be saved by utilizing a natural cold source such as low-temperature water (i.e., less than 15℃), cold air, snow, or ice.

As has been explained, PE is an application of CTES, and the key first step in developing the coupling cooling method. Moreover, although the implementation of CTES with an intermittent mode to enhance the energy storage performance is substantially significant work, it has not been studied. Thus, this study aims to improve the heat transfer performance of CTES by implementing an intermittent operational mode and evaluating the use of PE in a mine refuge chamber. A simplified numerical model of the intermittent cold storage of the surrounding rock is established, and the influence of the IR and IP on the cold storage performance in the refuge chamber is investigated in detail. In addition, long-term intermittent CTES is optimized, and an interchanging continuous/intermittent cold storage strategy is proposed. The results of this research are not only applicable to cold storage, as they can also be applied as a reference for yielding similar improvements in heat storage efficiency.

2. Model establishment

2.1 Parameter settings

In the current simulation, a typical 50-person refuge chamber is selected. The control parameters of the mine refuge chamber are listed in Table 2; the dimensionless storage temperature $\Theta = (t_{tcs}-t_a)/(t_0-t_a)$.

According to the following formula [17]:

$$r_c - r_i = 3.6\sqrt{a\tau} \tag{1}$$

the cooled-zone radius r_c, which is the heat transfer distance in SR, over a 96 h period is approximately 2 m. Thus, to meet the cold storage requirement of this study, $\Theta = 0.3$ for a 2-m-deep SR.

2.2 Simplification of boundary conditions

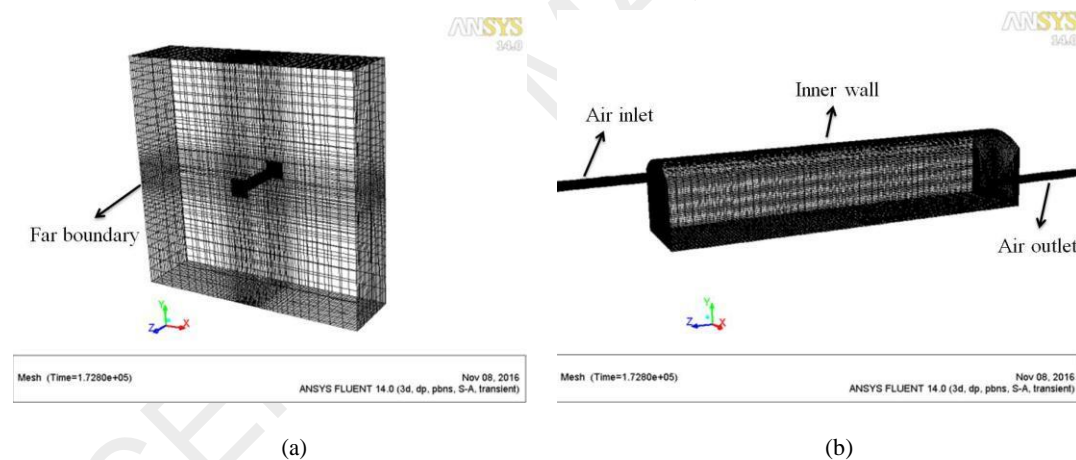(a)   (b)

Fig. 3. 3D numerical calculation mesh: (a) whole mesh; (b) chamber mesh.

In the pre-cooling stage, the influence of PCM devices on indoor air temperature is neglected because of the forced-air system. Thus, a 3D numerical model of a mine refuge chamber without PCM devices was developed by using ANSYS ICEM 14.0 and Fluent 14.0 software. The computation mesh is shown in Fig. 3. The refuge chamber with an air inlet and an air outlet was in the middle of the whole mesh. The SR was around the mine refuge chamber, and the inner wall was the interface between air and SR. The air was considered an incompressible Newtonian fluid

that flows in the form of a non-steady-state turbulence flow. The semi-implicit method for pressure-linked equations (SIMPLE) algorithm was implemented to describe the pressure-velocity coupling. The momentum and energy equations were both discretized using a second-order upwind difference scheme. The standard k-ε turbulence model was employed to calculate the turbulence flow. The far-boundary condition has been defined as a constant temperature condition in which the temperature is 20℃. Additionally, the inner wall of the SR is set as a coupled interface. A 1 s time step was applied, with the total number of steps being 172800. The number of grids was 5 million.
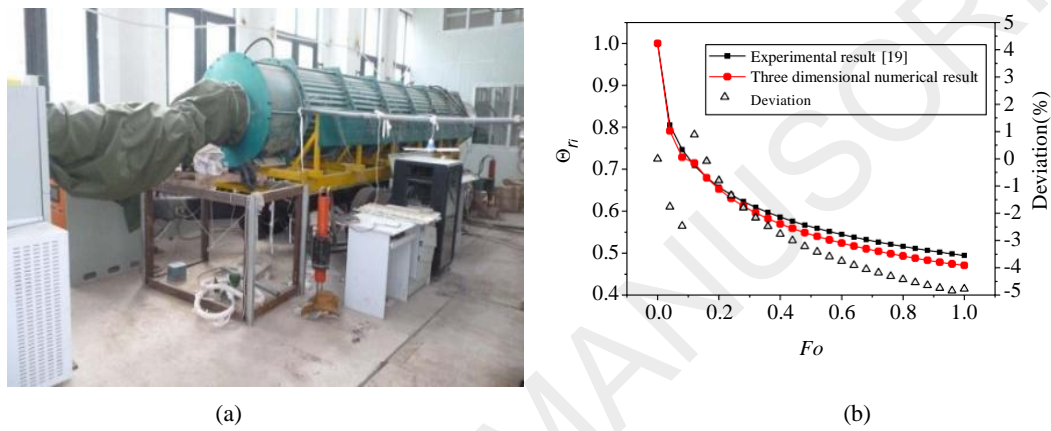

<div align="center">(a)   (b)</div>

<div align="center">Fig. 4. Experimental layout and comparison of the results:</div>

<div align="center">(a) experimental layout [19]; (b) comparison of the experimental and 3D numerical results.</div>

In order to verify the 3D numerical method for computing the ventilation in a cavern, the calculated result was compared to the experimental result of Zhang et al. [19], who conducted a theoretically similar experiment in a test tunnel. Fig. 4 (a) showed the experimental layout. The dimensions of the tunnel were $6 \times 0.1 \times 0.4$ m (length $\times$ internal diameter $\times$ outer diameter). The thermal diffusivity and conductivity of the SR were 0.8×10^{-6} m^2/s and 1.2 J/(m·K), respectively. The initial temperature of the tunnel was $T_0 = 30$℃. The air supply velocity and temperature were 5 m/s and $T_f = 20$℃, respectively, and the period of ventilation was 3.5 h. For more details on the test tunnel and instrumentations, refer to the paper by Zhang et al. [19].

Fig. 4 (b) presents a comparison of the simulated results of this study and the experimental results obtained by Zhang et al. [19]. Θ_{ri} is the dimensionless temperature calculated as $(T_{ri}-T_f)/(T_0-T_f)$ and the error curve was calculated as $\Delta\Theta_{ri}/\Theta_{ri,exp} \times 100\%$. The results show that the maximum difference in Θ_{ri} values is 0.024, and that the deviation is less than 5%. As can be seen, the 3D predicted results are in good agreement with the experimental results.
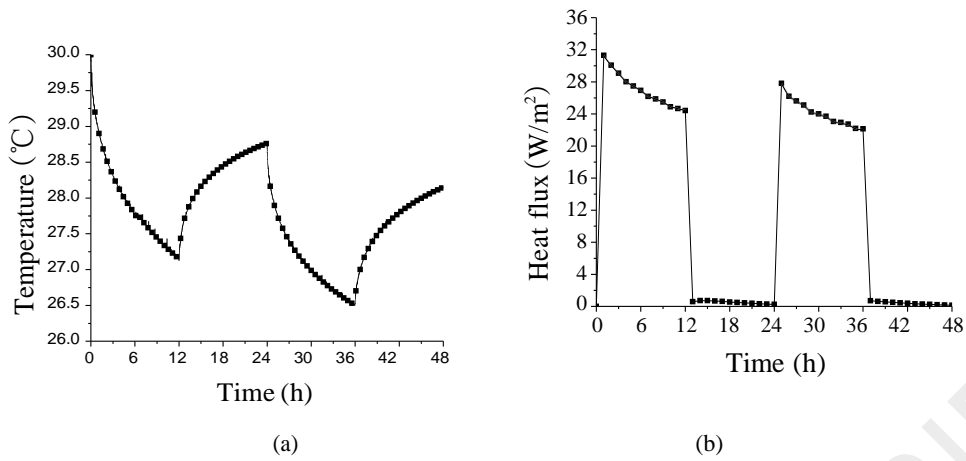
(a)	(b)

Fig. 5. 3D model of temperature and heat flux in the inner wall over 48 h:

(a)) temperature; (b) heat flux.

Fig. 5 illustrates the 3D-modeled variation in temperature and heat flux of the inner wall over a period of 48 h. Within a period of 24 h, the duration of operation is τ_{ope} = 12 h and the inactive period is τ_{ina} = 12 h. It can be seen from Fig. 5(a) that the temperature of the inner wall rapidly recovers during the standby period. Additionally, Fig. 5(b) shows that the heat flux during the standby period is significantly lower than that during active operation. Specifically, the average heat flux of each of the two durations of operation is 27 and 24 W/m^2, while that during the periods of standby is 0.51 and 0.39 W/m^2; this means that the heat flux during active operation is respectively 53 times and 62 times larger than that during inactivity.

Because the average heat flux during periods of standby is near zero, and thus significantly lesser than that observed during active operation, the heat transfer boundary condition applied the inner wall during periods of inactivity can be simplified as an adiabatic boundary condition. This simplification results in an approximately 2% error; however, by simplifying the boundary conditions, a one-dimensional (1D) model can be implemented.
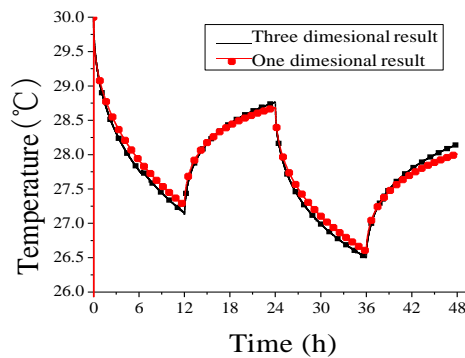

Fig. 6. Comparison of the 1D and 3D numerical results.

To verify the feasibility of the simplifying the system into a 1D numerical model by applying an adiabatic boundary condition to the standby mode, the results of calculations are compared with the 3D numerical results, as is shown in Fig. 6. The result shows no significant difference in temperature between the 1D and 3D numerical methods; this indicates that simplifying the standby system to an adiabatic process and implementing 1D numerical method will not significantly affect the model. Moreover, because it yields high computational and time costs, 3D numerical methods are not practical over extended periods. For these reasons, a simplified 1D numerical method is presented.

2.3 One-dimensional numerical model

By simplifying the boundary condition for the standby mode, the following assumptions regarding mine refuge chambers are employed to derive the governing equations [20-23]:

(i) The embedded depth of the refuge chamber exceeds 200 m, and the effects of ground temperature are neglected.

(ii) The ratio of the length to the width is larger than two, and the chamber is assumed to be a cylinder, as shown in Fig. 7. Additionally, $r_i = \sqrt{S / \pi} = 2$ m, where, r_i is the equivalent radius of the inner wall, and S is the area of the arched section.

(iii) The change in heat conduction along the depth gradient is assumed to be negligible because of the small temperature gradient.

(iv) The change in air temperature along the depth gradient is assumed to be negligible because of the short height of the cavern.

(v) The heat transfer caused by the moisture transfer through the rock is negligible.

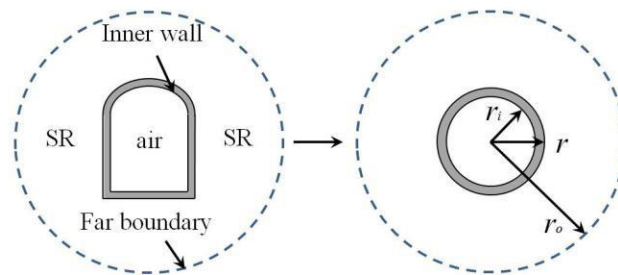(vi) The thermophysical property of the SR is assumed to be constant.

Fig. 7. Schematic of simplified mine refuge chamber: vertical mid-plane.

The equations for calculating changes in the temperature of the SR are as follows:

$$\frac{\partial T}{\partial \tau} = \alpha \left(\frac{\partial^2 T}{\partial r^2} + \frac{1}{r} \cdot \frac{\partial T}{\partial r} \right) \tag{2a}$$

$$\begin{cases} -\lambda_w \dfrac{\partial T(r,\tau)}{\partial r} = h_w \left[T_f - T(r_i, \tau) \right] & \tau \in \left(nIP, IR \times IP + n \times IP \right] \\[4mm] -\lambda_w \dfrac{\partial T(r_i,\tau)}{\partial r} = 0 & \tau \in \left(IR \times IP + n \times IP, (n+1)IP \right] \end{cases} \tag{2b}$$

$$T(r_\infty, \tau) = T_0 \tag{2c}$$

$$T(r,0) = T_0 \tag{2d}$$

where T is the temperature, T_0 is the initial temperature, τ is the time, α is the thermal diffusivity, r is the radius of the SR, r_i is the inner wall radius, λ_w is the thermal conductivity, T_f is the air temperature, r_∞ is the far boundary radius, IP is the time required to complete an operation-standby cycle, IR is the ratio of the inactive time τ_{ina} to the operating time τ_{ope}, n is a non-negative integer, and h_w is the natural convective heat-transfer coefficient between the air and inner wall, which is calculated via Eq. (3) [24]:

$$h_w = 6.76 \times v^{0.8} + 0.74 \tag{3}$$

The finite-volume method is used to discretize the functions. Fig. 8 shows the 1D computational grid of the SR. The basic discretized units are as follows:

$$\frac{\partial T}{\partial \tau} = \frac{T_i^k - T_i^{k-1}}{\Delta \tau}, \quad \frac{\partial T}{\partial r} = \frac{T_{i+1}^k - T_{i-1}^k}{2\Delta r}, \quad \frac{\partial^2 T}{\partial r^2} = \frac{T_{i+1}^k - 2T_i^k + T_{i-1}^k}{\Delta r^2} \tag{4}$$
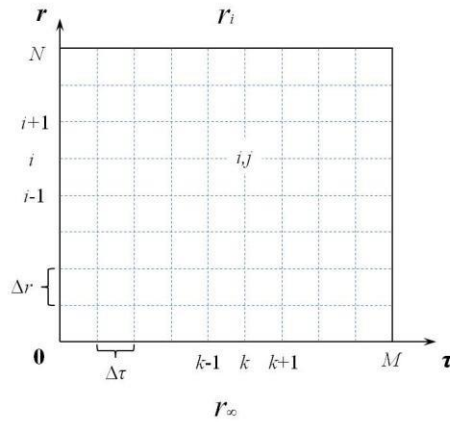

Fig. 8. 1D computational grid of SR.

The discretized results of Eqs. (2) and (4) are shown as Eq. (5). The temperature distribution

11

in the SR can be obtained via numerical calculations.

$$\begin{cases} T_i^{\,k} = T_0 & i = 0 \\ (\dfrac{Fo \times \Delta r}{2\,r_i} - Fo\,)T_{i-1}^{\,k} + (1 + 2\,Fo\,)T_i^{\,k} - (\,Fo\, + \dfrac{Fo \times \Delta r}{2\,r_i})T_{i+1}^{\,k} = T_i^{\,k-1} & i = 1 \sim N - 1 \end{cases} \quad (5a)$$

when $i=N$

$$\begin{cases} -2\,Fo \times T_{i-1}^{\,k} + (1 + 2\,Bi \times Fo\, + 2\,Fo\,)T_i^{\,k} = T_i^{\,k-1} + 2\,Fo \times Bi \times t_f \\ -2\,Fo \times T_{i-1}^{\,k} + (1 + 2\,Fo\,)T_i^{\,k} = T^{\,k-1} \end{cases}$$

$$\tau \in \left(nIP\,,\, IR \times IP + n \times IP\,\right]$$
$$\tau \in \left(\,IR \times IP + n \times IP\,,\,(n+1)\,IP\,\right] \qquad (5b)$$

where $Fo = \alpha \cdot \Delta\tau/(\Delta x)^2$ and $Bi = h_w \cdot \Delta x/\lambda_w$, which are the Fourier number and Biot number,

respectively; these numbers are implemented as parameters of the mesh size.
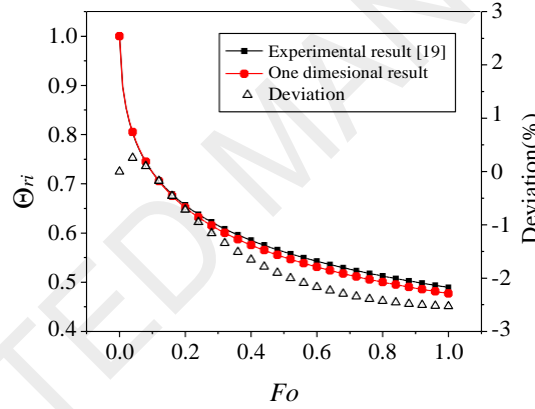
2.4 Model validation

Fig. 9. Comparison of 1D model results and experimental results of Zhang et al. [19].

To make the process of the model simplification more rigorous, after we proved the accuracy

of the 3D numerical model in Fig. 4, the calculated results of the simplified 1D model were

compared to the same experimental results of Zhang et al. [19] used to generate Fig. 4. Fig. 9

showed the comparison of the experimental and numerical results. The error curve was calculated

as $\Delta\Theta_{ri}/\Theta_{ri,exp} \times 100\%$. The results show that the maximum difference in Θ_{ri} is 0.012 and the

deviation is less than 3%. The 1D predicted results are in good agreement with the experimental

results; this confirms that this model is suitable for application in the current study.
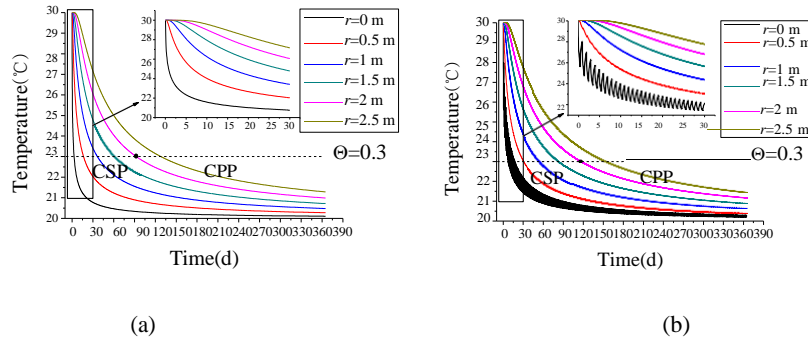
3. Results and discussion

Fig. 10. Rock temperature at varying distances from the inner wall over a period of 1 yr:

(a) continuous mode; (b) intermittent mode ($IR = 1$, $IP = 1$ d).

Fig. 10 shows the changes in rock temperature at six different depths ($r = 0$–2.5 m; interval = 0.5 m) over a period of 1 yr for two types of storage modes. Fig. 10(a) illustrates the results for the continuous mode. The most significant temperature decrease occurs within the first 30 days; this is followed by an increasingly gradual decrease in temperature with increases in depth and the days of operation. Fig. 10(b) illustrates the results for the intermittent mode. At $r = 0$ m, the temperature of the inner wall is observed to fluctuate in response to the intermittent operation; additionally, as time progresses, the amplitude of this fluctuation is observed to gradually decrease. As an example, the first-period temperature fluctuation of the inner wall is 4.4℃, while that of the last period is approximately 0.11℃. Furthermore, the amplitude of temperature fluctuation is also found to rapidly decrease with depth. This is evidenced by the following results: at $r = 0.5$ m, the amplitude of temperature fluctuation is very small, but as the depth is increased to $r = 1$ m, temperature fluctuation is no longer observed. This phenomenon occurs because the heat capacity of rock is large while its thermal conductivity is low; consequently, this generates a time lag and energy is attenuated as heat is transferred.

By comparing Figs. 10(a) and 10(b), it is found that the temperature variation observed during continuous and intermittent modes of operation exhibits identical trends at each depth. In addition, the temperature during the continuous mode of operation is observed as consistently lower than that observed during the intermittent mode; moreover, the difference in temperature between the two modes is observed to gradually decrease with time. More specifically, at 30, 60, 120, 180, 240, 300, and 360 d, the differences in inner wall temperature are 1.42, 0.90, 0.52, 0.37,

13

0.29, and 0.20℃, respectively.

The dimensionless target temperature $\Theta = 0.3$ is indicated in Fig. 10 (horizontal dashed line). It can be seen that the time required for the chamber temperature during continuous operation to reach the storage requirement is 92.5 d, while that of intermittent operation requires 116 d. Therefore, the entire cold storage process can be divided into two periods: the cold storage period (CSP) and the cold preservation period (CPP). To evaluate the energy consumption of the cold storage process, the net cold storage time τ_n is self-defined, which is expressed as

$$\tau_n = \tau_c \times \frac{1}{IR + 1} \tag{6}$$

where τ_c is the cold storage duration. Assuming that the energy consumption of the forced-air system operated in each day is the same, the net cold storage time τ_n can represent the energy consumption.

According to Eq. (6), τ_n values of the continuous and intermittent modes are 92.5 and 58 d, respectively. In this case, although, τ_{CSP}, the duration of the CSP is extended by 23.5 d as compared to the continuous mode, the net cold storage time of the intermittent mode is 34.5 d less than that of the continuous mode.

In order to shorten the τ_{CSP} and reduce the net cold storage time τ_n, it is necessary to analyze impact of the influential factors, which include the intermittent ratio and intermittent period. It should be noted that only the parameter of interest is varied when evaluating the effects on temperature.

3.1 Effects of intermittent ratio

As previously mentioned, the intermittent ratio (IR) is the ratio of inactive time to operating time in a single period, which can be calculated as $IR = \tau_{ina} / \tau_{ope}$; it is also one of the most significant parameters in intermittent operation. In order to investigate the influence of the IR on rock temperature during the cold storage process over a period of 1 yr, all remaining parameters are kept constant. Accordingly, the IP is set to 1 d, and the IR is set to vary as follows: 0, 0.2, 0.5, 1, 2, and 5.
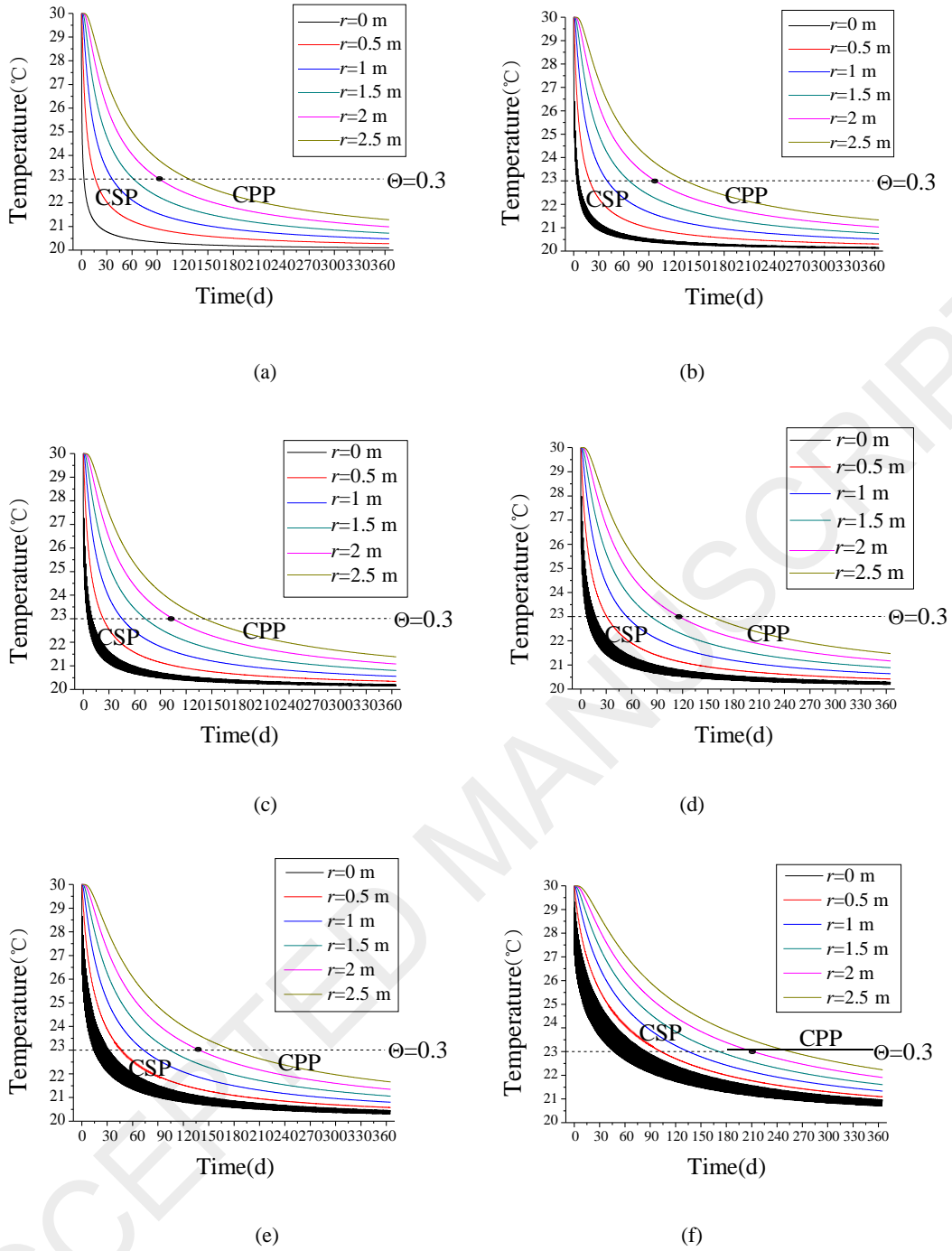
14

Fig. 11. Rock temperature over a period of 1 yr for various *IR*s: (a) *IR* = 0 (continuous mode);
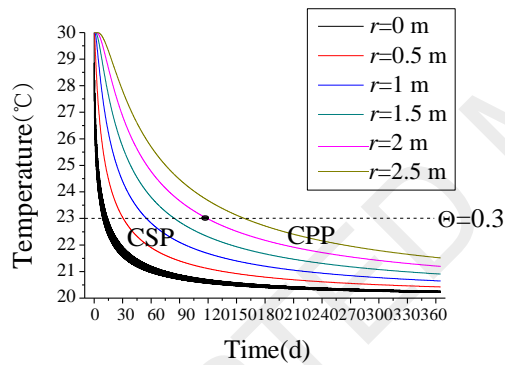
(b) *IR* = 0.2; (c) *IR* = 0.5; (d) *IR* = 1; (e) *IR* = 2; (f) *IR* = 5.

Fig. 11 illustrates the changes in rock temperature over a period of 1 yr for various *IR*s. The results show that, with increasing *IR*, the amplitude of inner wall temperature fluctuation is increased and the speed to store cold is reduced. Specifically, as the *IR* increases from 0 to 5, the τ_{CSP} increases as follows: 92.5, 97.8, 104.5, 116, 139.1, and 211.5 d, and according to Eq. (6), $\tau_{n,CSP}$, the net cold storage time in CSP decreases as follows: 92.5, 81.5, 69.7, 58, 46.4, and 35.3 d. These

15

results indicate that increasing the *IR* results in an extended τ_{CSP} and less energy consumption. The reason for this relationship could be that, while keeping the *IP* constant, as the *IR* is increased, the duration of operation will decrease, thereby necessitating an extended τ_{CSP}. Furthermore, because the corresponding time of inactivity will increase, the storage efficiency may improve, thereby causing energy consumption to decrease.

### 3.2 Effects of intermittent period

As previously mentioned, the intermittent period (IP) is the time required to complete an operation-standby cycle, which can be calculated as $IP = \tau_{ina} + \tau_{ope}$, and it is also one of the most significant parameters in intermittent operation. To investigate the influence of the *IP* on rock temperature during the cold storage process over a period of 1 yr, all other parameters are kept constant. Accordingly, the *IR* is set to 1, and the *IP* is set to vary as follows: 0.25, 0.5, 1, 2, 4, 7, and 15 d.
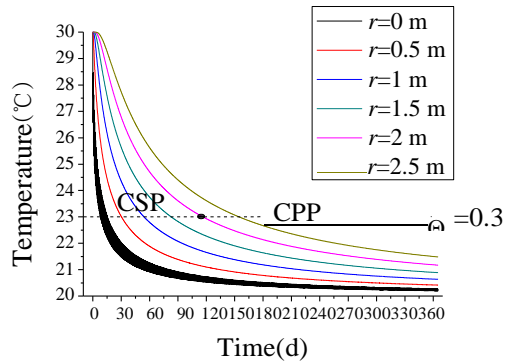

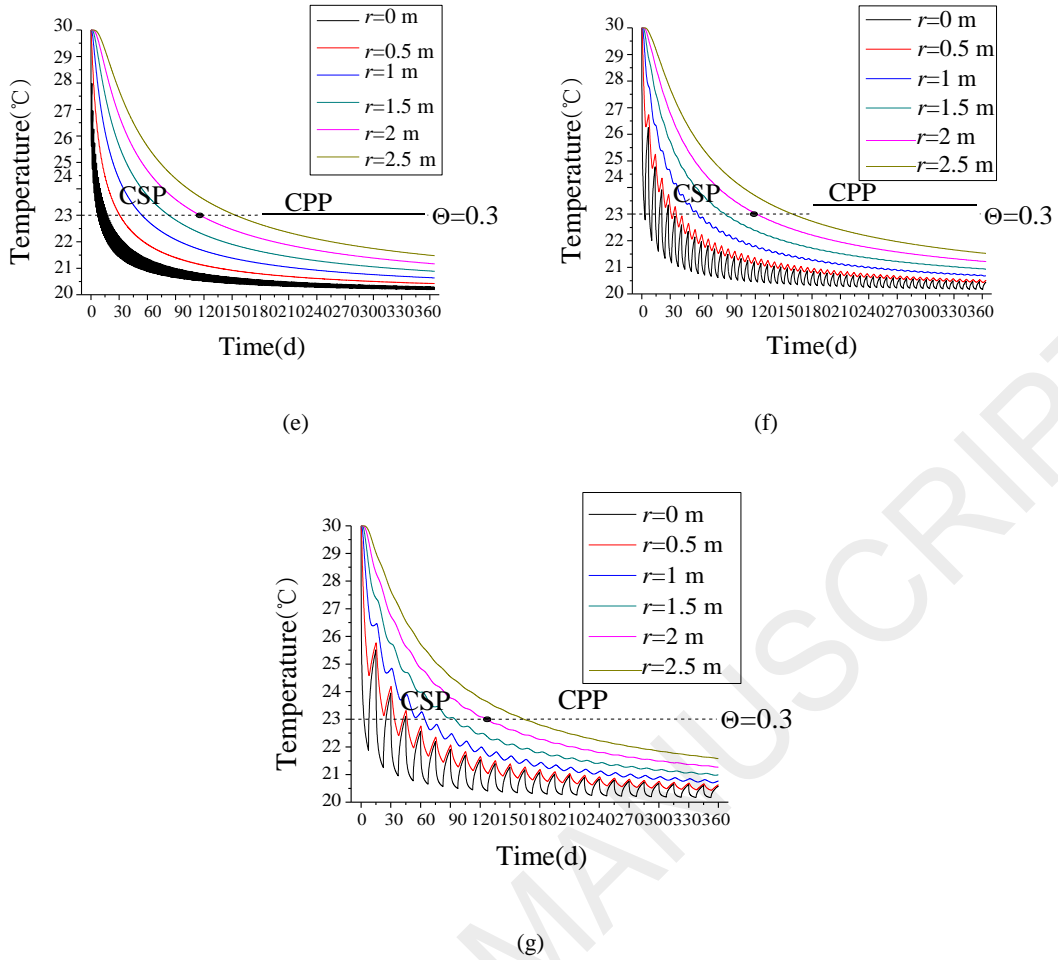(a)   (b)
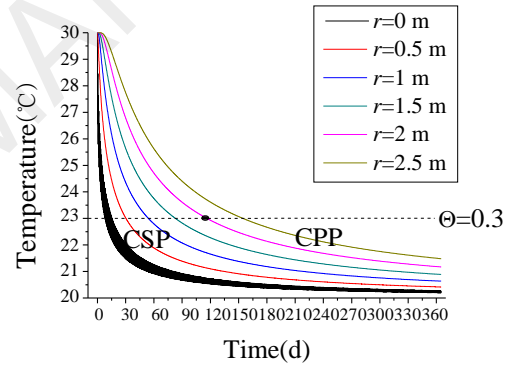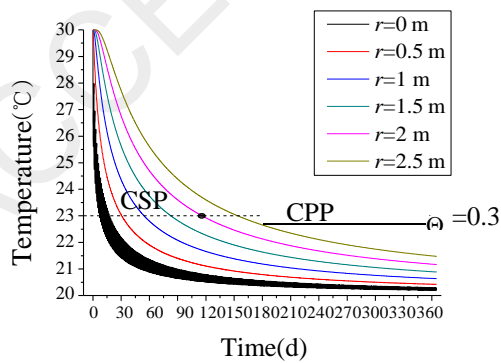
(c)   (d)

(e)

(f)

(g)

Fig. 12. Rock temperature over a period of 1 yr for various *IP*s: (a) *IP* = 0.25 d; (b) *IP* = 0.5 d; (c) *IP* = 1 d; (d) *IP* = 2 d; (e) *IP* = 4 d; (f) *IP* = 7 d; (g) *IP* = 15 d.

Fig. 12 shows the changes in rock temperature over a period of 1 yr for various *IP*s. The results show that, with increasing *IP*, the amplitude of the inner wall temperature fluctuation is increased, and the cold storage speed exhibits a decreasing-increasing trend. Specifically, as the *IP* is increased from 0.25 to 15 d, the τ_{CSP} varies as follows: 119, 116.4, 116, 116.8, 118.9, 121.3, and 127.4 d, and as according to Eq. (6), the $\tau_{n,CSP}$ varies as follows: 59.5, 58.2, 58, 58.4, 59.5, 60.7, and 63.7 d. The reason for this relationship could be that, when the *IP* is small, the effects of wall temperature recovery are not evident. However, when the *IP* is increased to approximately 1 d, the effects of the increased wall temperature gradually become more significant; as these conditions are favorable for heat transfer, the shortest τ_{CSP} is observed. If the *IP* is further increased, the rate of heat recovery of the rock will decrease, thereby causing the $\tau_{n,CSP}$ to decrease. Although it exhibits moderate fluctuation, varying the *IP* does not yield significant fluctuation in the τ_{CSP} because the *IR* remains constant. This is evidenced in the results: as the *IP* is increased from 1 to

17

15 d, the increase in the τ_{CSP} does not exceed 10%.

3.3 Control strategy for CTES for continuous and intermittent operation

3.3.1 Control strategy for the CSP

To ensure the safety of the miners, it is necessary to store cold as quickly as possible. Therefore, the evaluation indices for the CSP include a time evaluation index τ_{CSP}, which is the duration time of CSP, and energy consumption evaluation index $\tau_{n,CSP}$, which is the net cold storage time of CSP. According to the sensitivity analyses presented in preceding sections, it can be determined that the *IR* and *IP* yield different effects on the cold storage performance of CTES; thus, there is a need to accordingly adjust both the *IR* and *IP* to increase efficiency.
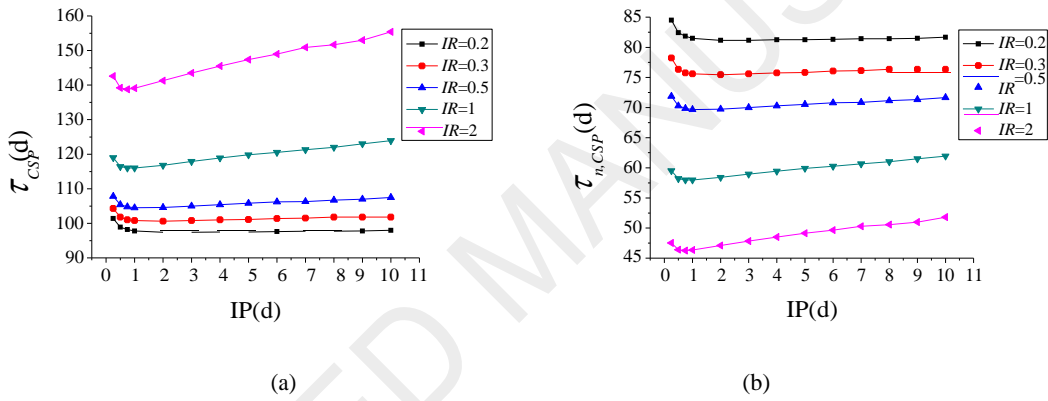

(a)   (b)

Fig. 13. τ_{CSP} and $\tau_{n,CSP}$ as a function of the *IP* for various *IR*s: (a) τ_{CSP}; (b) $\tau_{n,CSP}$.

Fig. 13 shows the τ_{CSP} and $\tau_{n,CSP}$ each as a function of the *IP* for various *IR*s. The results indicate that both τ_{CSP} and $\tau_{n,CSP}$ have a similar tendency to initially decrease and then increase as the *IP* increases; moreover, this trend becomes more pronounced as the *IR* increases. It should also be noted that the τ_{CSP} increases with increasing *IR*, while the $\tau_{n,CSP}$ decreases.

In order to comprehensively evaluate the increased efficiency with respect to time and energy, a dimensionless index φ is proposed; this index takes into account the τ_{CSP} and $\tau_{n,CSP}$ to characterize the energy saved by prolonging unit time in the intermittent mode. It is calculated as follows:

$$\varphi = \frac{\tau_{n0,CSP} - \tau_{n,CSP}}{\tau_{CSP} - \tau_{CSP0}} \tag{7}$$

where $\tau_{n0,CSP}$ corresponds to the $\tau_{n,CSP}$ for continuous operation, and τ_{CSP0} corresponds to the τ_{CSP} for continuous operation. Larger values of φ result in more energy saved by prolonging unit time;

18

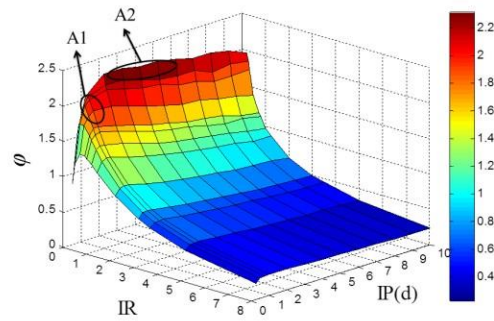consequently, the process of energy saving becomes more efficient.

Fig. 14. φ as a function of various intermittent periods and ratios.

Fig. 14 illustrates the variation in φ according to the *IR* and *IP*. Two distinct peaks can be observed with respect to the *IP*. Specifically, when the *IP* is between 0.5 and 2 d, the φ peak appears in the A1 region, and the *IR* is between 0.3 and 1; when the *IP* is between 2 and 6 d, the φ peak appears in the A2 region and the *IR* is 0.1. The results from the intermittent mode with the *IP* between 2 and 6 d and *IR* = 0.1 in the A2 region are comparable to those of the continuous mode; thus, the continuous mode can represents the intermittent mode of the A2 region.

Therefore, a continuous mode or intermittent mode with *IR* = 0.3–1 and *IP* = 0.5–2 d are suggested for implementation to maximize efficiency during the CSP. As compared to that observed during continuous operation, during intermittent operation the τ_{CSP} is extended by 10–26%, while the energy consumption is reduced by 17–37%.

3.3.2 .2 Control strategy for the CPP

The cold preservation period (CPP) refers to the long-term cold preservation process following the completion of cold storage; this process is essential to avoid the temperature (heat) recovery of rock caverns. In this study, the CPP is evaluated to determine the optimal conditions for convenience and energy saving. Therefore, the evaluation indices for the CPP include an intermittent period evaluation index *IP* and energy consumption evaluation index $\tau_{n,CPP}$. An intermittent mode with *IR* = 1 and *IP* = 1 d is implemented in the CSP calculations.
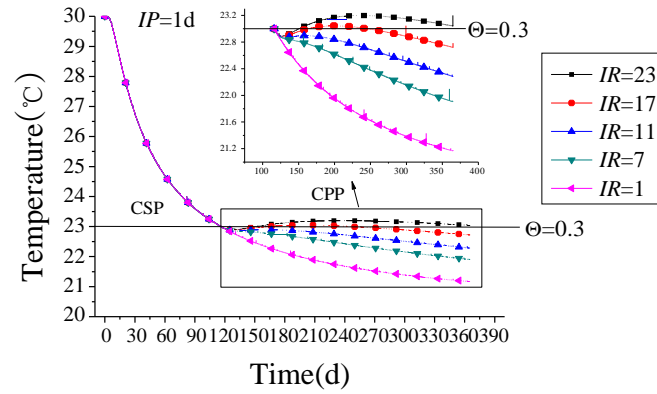
Fig. 15. Rock temperature at $r = 2$ m for various IRs during the CPP.

Fig. 15 shows the change in rock temperature at $r = 2$ m for various IRs during the CPP. The results demonstrate that increasing the IR will increase the temperature during the CPP. Specifically, when the IR is less than or equal to 11, the rock temperature during the CPP remains below the control temperature; however, when the IR is greater than or equal to 17, the temperature during the CPP exceeds the control temperature. This trend occurs because an increase in the IR indicates an increase in the duration of inactivity, thereby allotting more time for temperature recovery. Although a larger IR can conserve a greater amount of energy, a maximum IR should be established to prevent the SR temperature from progressively increasing.
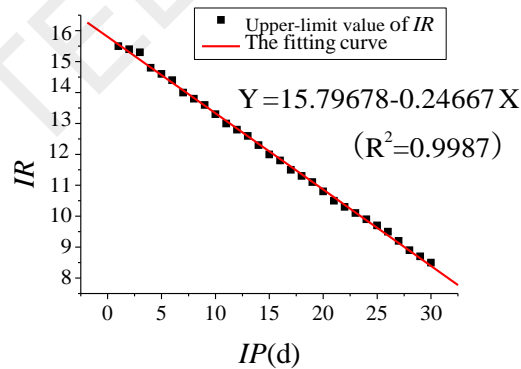

Fig. 16. Upper-limit IR values as a function of IP.

Fig. 16 shows the upper-limit IR values for different IPs. From this figure, it can be seen that larger IPs correspond to lower upper-limit IR values; in addition, a linear relationship between IR and IP can be observed. This linear relationship is defined as follows:

$$IR_{Upper} = -0.24667 \, IP + 15.79678 \qquad (R^2 = 0.9987) \qquad (8)$$

According to Eq. (8), $IR_{Upper} = 0$ when $IP = 64$, indicating that once IP exceeds 64 d, the temperature of the surrounding rock will exceed the control temperature; moreover, this will occur irrespective of the IR. Thus, the upper-limit of the IP is set as 64 d.
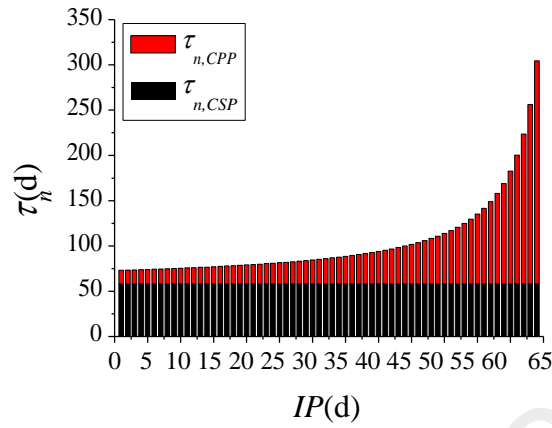

Fig. 17. $\tau_{n,CPP}$ and total net duration of cold storage as functions of IP over a period of 1 yr.

Fig. 17 illustrates the respective relationships between IP and $\tau_{n,CPP}$ and IP and the total net duration of cold storage over a period of 1 yr, as according to Eqs. (6) and (8). The total net duration of cold storage is equal to the sum of $\tau_{n,CPP}$ and $\tau_{n,CSP}$. The results indicate that the initial value of $\tau_{n,CSP}$ (58 d) is unchanged because the conditions of the intermittent mode (i.e., $IR = 1$ and $IP = 1$ d) remain constant throughout the CSP. Conversely, during the CPP, $\tau_{n,CPP}$ is observed to progressively increase with the increase of IP and corresponding IR. This trend is also observed in the total net duration of cold storage. More specifically, as IP is increased from 1 to 20 d, 21 to 41 d, and 42 to 64 d, the total net period of cold preservation is found to increase from 73 to 78 d, 79 to 95 d, and 97 to 304 d, respectively. Based on the intermittent period evaluation index IP and energy consumption evaluation index $\tau_{n,CPP}$, $IP = 20$ d is determined to yield the highest efficiency; in addition, by implementing this value of IP into Eq. (8), it is found that the corresponding IR is 11. These results thus indicate that the optimal parameters for the CPP with applied intermittent mode are $IR = 11$ and $IP = 20$ d. Additionally, as compared to the continuous mode, the intermittent mode can save 92% more energy.

As optimization of each period requires different intermittent mode, it is suggested to adjust the parameters accordingly throughout the entire cold storage process of the cavern envelope. Under the current background conditions, a continuous mode or intermittent mode of operation in which $IR = 0.3–1$ and $IP = 0.5–2$ d is suggested for implementation during the CSP, while an

21

intermittent mode with $IR = 11$ and $IP = 20$ d is suggested for the CPP.

When a continuous mode during the CSP and an intermittent mode with $IR = 11$ and $IP = 20$ d during the CPP are in the implementation, the duration of the CSP is $\tau_{CSP} = 92.5$ d, and the net cold storage time in 1 yr is 115.2 days, which can be calculated as

$$\tau_n = \tau_{n,CSP} + \tau_{n,CPP}$$

$$= \tau_{CSP} \times \frac{1}{IR_{CSP} + 1} + \tau_{CPP} \times \frac{1}{IR_{CPP} + 1} \tag{10}$$

As compared to the conventional continuous mode, the CSP duration is the same, but the net cold storage time is reduced by 249.8 days, which means the energy consumption of cold storage is reduced by 68% in 1 yr.

When an intermittent mode with $IR = 1$ and $IP = 1$ d during the CSP and an intermittent mode with $IR = 11$ and $IP = 20$ d during the CPP are in the implementation, the duration of the CSP is $\tau_{CSP} = 116$ d, and the net cold storage time in 1 yr is 78.8 days according to Eq. (10). As compared to the conventional continuous mode, although the CSP duration is extended by 26%, the net cold storage time is reduced by 286.2 days, which means the energy consumption is reduced by 78% in 1 yr.

In a summary, as compared to the conventional continuous mode, the CSP duration is extended by 0–26%, and the energy consumption of cold storage is reduced by 68–78% in 1 yr when an optimized interchanging continuous/intermittent cold storage strategy is in the implementation.

4. Conclusions

This study aims to improve the heat transfer performance of CTES by implementing an intermittent operational mode. A simplified numerical simulation model of the intermittent cold storage of the rock surrounding a mine refuge chamber was established. Next, the effects of the IR and IP on cold storage performance were investigated. In addition, long-term CTES with an applied intermittent mode has been optimized, and an interchanging continuous/intermittent cold storage strategy has been proposed. The conclusions have been summarized as follows:

(1) Temperature fluctuation is observed in the inner wall under intermittent operating conditions; the amplitude of this fluctuation is observed to gradually decrease with time and depth. The intermittent ratio and intermittent period differently influence the long-term storage of a cavern envelope. As the *IR* is increased, the CSP duration is progressively prolonged; however, as the *IP* is increased, the CSP duration exhibits a decreasing-increasing trend. Furthermore, the simulation results indicate that *IR* yields the most significant effect on energy consumption.

(2) The cold storage process is divided into two phases: CSP and CPP. In the CSP, a dimensionless index φ is proposed; this index takes into account both τ_{CSP} and $\tau_{n,CSP}$, which have the ability to characterize the energy saved according to the prolonged unit time when an intermittent mode is implemented. In the CPP, to prevent temperature recovery of the surrounding rock, the method for determining an *IP*-dependent upper limit value for *IR* is established.

(3) Reasons for implementing an interchanging strategy in the cold storage process of a cavern envelope are presented. A continuous mode or intermittent mode of operation in which *IR* = 0.3–1 and *IP* = 0.5–2 d is suggested for implementation during the CSP, while an intermittent mode with *IR* = 11 and *IP* = 20 d is suggested for the CPP. As compared to the conventional continuous mode, the CSP duration is extended by 0–26%, and the energy consumption of cold storage is reduced by 68–78% within 1 yr.

This study demonstrates that an optimized intermittent mode can significantly reduce the energy consumption and facilitate regulation of the cold storage process without extensively prolonging the storage time. Furthermore, this strategy is not only applicable to cold storage but can also be implemented as a reference for yielding similar improvements in heat storage efficiency.

Acknowledgements

References

[1] Navarro L, Gracia AD, Colclough S, Browne M, McCormack SJ, et al. Thermal energy storage in building integrated thermal systems: A review. Part 1. active storage systems. Renew Energy. 2016;88:526-547.

[2] Navarro L, Gracia AD, Niall D, Castell A, Browne M, et al. Thermal energy storage in building integrated thermal systems: A review. Part 2. Integration as passive system. Renew Energy. 2016;85:1334-1356.

[3] Miró L, Oró E, Boer D, Cabeza LF. Embodied energy in thermal energy storage (TES) systems for high temperature applications. Appl Energy. 2015;137:793-799.

[4] Miró L, Gasia J, Cabeza LF. Thermal energy storage (TES) for industrial waste heat (IWH) recovery: A review. Appl Energy. 2016;179:284-301.

[5] Park JW, Park D, Ryu DW, Choi BH, Park ES. Analysis on heat transfer and heat loss characteristics of rock cavern thermal energy storage. Eng Geol. 2014;181:142-156.

[6] Ghoreishi-Madiseh SA, Sasmito AP, Hassani FP, Amiri L. Performance evaluation of large scale rock-pit seasonal thermal energy storage for application in underground mine ventilation. Appl Energy. 2017;185:1940-1947.

[7] Xu J, Li Y, Wang RZ, Liu W. Performance investigation of a solar heating system with underground seasonal energy storage for greenhouse application. Energy. 2014;67:63-73.

[8] Shang Y, Li S, Li H. Analysis of geo-temperature recovery under intermittent operation of ground-source heat pump. Energy Build. 2011;43:935-943.

[9] Kojo A, Jong MC. Current status of the performance of GSHP (ground source heat pump) units in the Republic of Korea. Energy. 2012;47:77-82.

[10] Cao X, Yuan Y, Sun L, Lei B, Yu N, et al. Restoration performance of vertical ground heat exchanger with various intermittent ratios. Geothermics. 2015;54:115-121.

[11] Yuan Y, Cao X, Wang J, Sun L. Thermal interaction of multiple ground heat exchangers under different intermittent ratio and separation distance. Appl Therm Eng. 2016;108:277-286.

[12] Liu L, Yu Z, Zhang H, Yang H. Performance improvements of a ground sink direct cooling system under intermittent operations. Energy Build. 2016;116:403-410.

[13] Faizal M, Bouazza A, Singh RM. An experimental investigation of the influence   of

intermittent and continuous operating modes on the thermal behaviour of a full scale geothermal energy pile. Geomechanics Energy Environ. 2016;8:8-29.

[14] Shang Y, Dong M, Li S. Intermittent experimental study of a vertical ground source heat pump system. Appl Energy. 2014;136:628-635.

[15] Zhang Z, Yuan Y, Wang K, Gao X, Cao X. Experimental investigation on influencing factors of air curtain systems barrier efficiency for mine refuge chamber. Process Saf Environ Prot. 2016;102:534-546.

[16] Zhang Z, Yuan Y, Wang K. Effects of number and layout of air purification devices in mine refuge chamber. Process Saf Environ Prot. 2017;105:338-347.

[17] Yuan Y, Gao X, Wu H, Zhang Z, Cao X, et al. Coupled Cooling Method and Application of Latent Heat Thermal Energy Storage Combined with Pre-cooling of Envelope: Method and Model Development. Energy. 2017;119:817-833.

[18] Gao X, Yuan Y, Cao X, Wu H, Zhao X, et al. Coupled cooling method and application of latent heat thermal energy storage combined with pre-cooling of envelope: Sensitivity analysis and optimization. Process Saf Environ Prot. 2017;107:438-453.

[19] Zhang Y, Wan Z, Gu B, Zhou C. An experimental investigation of transient heat transfer in surrounding rock mass of high geothermal roadway. Therm Sci. 2016:53-53.

[20] Szabó J, Kajtár L, Nyers J, Bokor B. A new approach and results of wall and air temperature dynamic analysis in underground spaces. Energy. 2016;106:520-527.

[21] Xiao Y, Liu X, Zhang R. Calculation of transient heat transfer through the envelope of an underground cavern using Z-transfer coefficient method. Energy Build. 2012;48:190-198.

[22] Yuan Y, Cheng B, Mao J, Du Y. Effect of the thermal conductivity of building materials on the steady-state thermal behavior of underground building envelopes. Build Environ. 2006;41:330-335.

[23] Yuan Y, Ji H, Du Y, Cheng B. Semi-analytical solution for steady-periodic heat transfer of attached underground engineering envelope. Build Environ. 2008;43:1147-1152.

[24] Gillies ADS, Creevy P, Danko G, Moussetjones PF. Determination of the in situ mine surface heat transfer coefficient. In: Proceedings of Fifth US Mine Ventilation Symposium. 1991:288-298.

Table captions

Table 1. Evaluation and application of four conventional cooling methods.

Table 2. Parameters for simulation of a mine refuge chamber and ventilation.

Figure captions

Fig. 1. Interior of a typical permanent refuge chamber.

Fig. 2. Schematic of proposed coupled cooling method: (a) PE during peacetime; (b) heat storage
of LHTES and envelope during working time.

Fig. 3. 3D numerical calculation mesh: (a) whole mesh; (b) chamber mesh.

Fig. 4. Experimental layout and comparison of the results: (a) experimental layout [19];
(b) comparison of the experimental and 3D numerical results.

Fig. 5. 3D model of temperature and heat flux in the inner wall over 48 h: (a) temperature; (b) heat
flux.

Fig. 6. Comparison of the 1D and 3D numerical results.

Fig. 7. Schematic of simplified mine refuge chamber: vertical mid-plane.

Fig. 8. 1D computational grid of SR.

Fig. 9. Comparison of calculated 1D results and experimental results of Zhang et al. [19].

Fig. 10. Rock temperature at varying distances from the inner wall over a period of 1 yr: (a)
continuous mode; (b) intermittent mode ($IR = 1$, $IP = 1$ d).

Fig. 11. Rock temperature over a period of 1 yr for various IRs: (a) $IR = 0$ (continuous mode);   (b)
$IR = 0.2$; (c) $IR = 0.5$; (d) $IR = 1$; (e) $IR = 2$; (f) $IR = 5$.

Fig. 12. Rock temperature over a period of 1 yr for various IPs: (a) $IP = 0.25$ d; (b) $IP = 0.5$ d; (c)
$IP = 1$ d; (d) $IP = 2$ d; (e) $IP = 4$ d; (f) $IP = 7$ d; (g) $IP = 15$ d.

Fig. 13. τ_{CSP} and $\tau_{n,CSP}$ as a function of the IP for various IRs: (a) τ_{CSP}; (b) $\tau_{n,CSP}$.

Fig. 14. φ as a function of various intermittent periods and ratios.

Fig. 15. Rock temperature at $r = 2$ m for various IRs during the CPP.

Fig. 16. Upper-limit IR values as a function of IP.

Fig. 17. $\tau_{n,CPP}$ and total net duration of cold storage as functions of IP over a period of 1 yr.

Tables

Table 1. Evaluation and application of four conventional cooling methods.

Cooling methods	Advantages	Disadvantages	Application
CO_2 phase-change cooling	Operable without electrical power; Highly stable	Risk of leakage; Requires regular inspection and replacement; Difficult to maintain	Mine with ambient temperature below 31℃
Explosion-proof air conditioning	Excellent cooling effect; Convenient adjustment	Gas explosion may render refrigerator inoperative; Requires an intrinsically safe high-power battery	Metallic/ nonmetallic mine
Ventilation cooling	No safety hazard; Air purification function	Ventilation ducts susceptible to damage; Poor cooling effect at increased depths	Shallow mine
Ice storage cooling	No safety hazard; Highly stable	Compressor is easily eroded; High maintenance cost; Large size; Requires a fan	Any conditions

Table 2. Parameters for simulation of a mine refuge chamber and ventilation.

Symbol	Description	Value
L_R	Refuge chamber length	17 m
W_R	Refuge chamber width	4 m
H_{R1}	Side wall height	2.8 m
H_{R2}	Vault height	3.5 m
r_∞	Far boundary	50 m
ρ	SR density	2400 kg/m^3
c_P	SR specific heat	902 J/(kg·K)
λ	SR thermal conductivity	2 W/(m·K)
t_0	Initial temperature	30℃
t_f	Air temperature	20℃
t_{tcs}	Target cold storage temperature	23℃
Θ	Dimensionless target cold storage temperature	0.3
v	Indoor wind speed	2 m/s